

## Accepted Manuscript

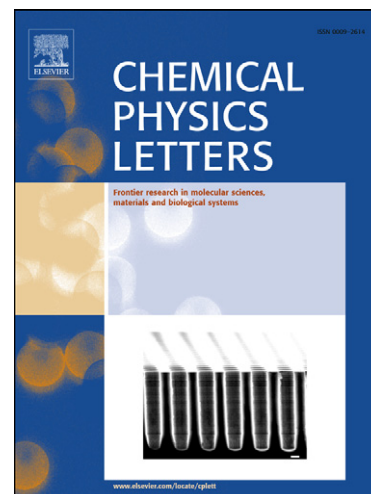
Surface-Enhanced Raman Scattering from small numbers of single-walled carbon nanotubes and oxidised single-walled carbon nanotubes

Nebras Al-Altar, Eamonn Kennedy, Ilona Kopf, Silvia Giordani, James H. Rice

PII: S0009-2614(12)00257-6  
DOI: [10.1016/j.cplett.2012.02.052](https://doi.org/10.1016/j.cplett.2012.02.052)  
Reference: CPLETT 30090

To appear in: *Chemical Physics Letters*

Received Date: 2 December 2011  
Accepted Date: 19 February 2012



Please cite this article as: N. Al-Altar, E. Kennedy, I. Kopf, S. Giordani, J.H. Rice, Surface-Enhanced Raman Scattering from small numbers of single-walled carbon nanotubes and oxidised single-walled carbon nanotubes, *Chemical Physics Letters* (2012), doi: [10.1016/j.cplett.2012.02.052](https://doi.org/10.1016/j.cplett.2012.02.052)

This is a PDF file of an unedited manuscript that has been accepted for publication. As a service to our customers we are providing this early version of the manuscript. The manuscript will undergo copyediting, typesetting, and review of the resulting proof before it is published in its final form. Please note that during the production process errors may be discovered which could affect the content, and all legal disclaimers that apply to the journal pertain.

# Surface-Enhanced Raman Scattering from small numbers of single-walled carbon nanotubes and oxidised single-walled carbon nanotubes

Nebras Al-Altar<sup>1</sup>, Eamonn Kennedy<sup>1</sup>, Ilona Kopf<sup>2</sup>, Silvia Giordani<sup>2</sup>, James H Rice<sup>1</sup>

<sup>1</sup> *School of Physics, University College Dublin, Belfield, Dublin 4, Ireland*

<sup>2</sup> *School of Chemistry/CRANN, Trinity College Dublin, Dublin 2, Ireland*

## Abstract

Temporal fluctuations of surface-enhanced Raman scattering spectra of purified and oxidised single walled carbon nanotubes have been observed. SERRS spectra were recorded that possessed fluctuating spectral profiles, these profiles possessed randomly fluctuation peak intensities and positions. Observation of bands in the 1000 to 1200  $\text{cm}^{-1}$  frequency window was observed. A series of peaks in this window were observed to coincide with peak positions that have been assigned to arise from Stone-Thrower-Wales and heptagonal-pentagonal intramolecular junction defects on the nanotubes surface. We find that these peaks also occur for chemically treated SWCNTS.

## 1. Introduction

Single-walled carbon nanotubes (SWCNT) have attracted considerable research effort in understanding and applying their properties [1,2]. One way of tailoring the electronic properties of carbon nanotubes is to add chemical groups to the carbon nanotube [2-4]. The addition of a chemical group via covalent bonding alters the conjugative network of the graphene sheet and creates changes in the electronic structure of the SWCNT. In addition to this the exposure to chemical treatments potentially results in the displacement of carbon atoms from graphite network creating vacancies [5-8]. The effect of adding chemical groups to the surface of the nanotube potentially enhances such properties as field emission, chemical detection sensitivity and electrochemical capacity as well as interface interactions between the nanotube surface and other materials or surfaces [9,10].

Surface enhanced Raman scattering (SERRS) can enhance the Raman signal of SWCNTs by up to 14 orders of magnitude [1,11-13]. SERRS can occur when the SWCNT is placed in contact with metallic (such as silver or gold) nanostructured materials [12,13]. These nanomaterials enable enhancement via localised optical fields. The size of these localised regions can be on the order of 5 nm. This enables small numbers of nanotubes to be probed down to the single nanotube level [12-14]. Raman spectroscopy is able to detect the presence of topological defects on SWCNT. Raman spectroscopy enables characterization of alternations in the graphene network though monitoring the Raman D band. This band assigned to a phonon mode originates from the hexagonal structure of graphite [1,12-14], whereby the presence of pentagon, heptagon, and octagon configurations in place of the hexagonal structure is referred to as topological defects [5,7,8].

The presence of defects in SWCNTs has implications for their application. This has motivated the characterization of defects such as topological defects in SWCNTs. One such topological defect are adjacent pentagon/heptagon pairs, called Stone-Thrower-Wales (STW) and heptagonal-pentagonal intramolecular junction defects [7,8]. As outlined by Miyamoto et al a STW defect consists of a localised  $\pi/2$  rotation of a C-C bond, such that two pentagons and heptagons are created [15]. These pentagon and heptagon arrangements potentially translocate along the structure, creating either dislocation centres in regions of positive

1 (pentagons) or negative (heptagons) Gaussian curvature, which ultimately lead to the closing  
2 of the nanostructure. A limited number of studies have been performed applying Raman  
3 spectroscopy to study defects on SWCNTs. The presence of STW defects changes the  
4 structural symmetry of the SWCNT and consequently vibrational modes associated with the  
5 topological defects are expected. Fujimori et al reported temporally fluctuating SERRS  
6 spectra from SWCNTs [8]. The authors applied SERRS to detect STW defects in SWCNTs.  
7 Temporally fluctuating spectra in SERRS occurred with additional peaks not observed in the  
8 non-SERRS spectra. These peaks were assigned to dynamic reconstruction of defective  
9 structures of SWCNTs arising from STW defects in the vicinity of SERRS-active sites under  
10 irradiation of the laser light.  
11

12  
13 Here we perform SERRS studies on commercially sourced SWCNTs and purified SWCNTs  
14 that have been chemically treated to improve their purity and also to alter the structure of the  
15 nanotube surface via covalently attaching carboxylic acid groups [4]. The purification process  
16 removing impurities such as graphene or fullerenes which may be present in untreated  
17 SWCNT samples. This aide's definitive assignment of the observed Raman peaks as such  
18 impurities potentially possess Raman active peaks that overlap with peaks associated with  
19 defects. SWCNTs with chemical groups covalently to the SWCNT surface were investigated  
20 assessing the impact of altering the electronic arrangement of the nanotube surface. The  
21 presence of structural changes in the SWCNT in the vicinity of SERRS-active sites (namely  
22 STW defects) has been asserted here to explain the occurrence of bands observed in the  
23 SERRS spectrum of purified SWCNT via comparison with reported theoretical calculated  
24 band positions for defects [7,8]. SERRS spectra were recorded that possessed fluctuating  
25 spectral profiles, these profiles possessed randomly fluctuation peak intensities and positions.  
26 Observation of bands in the  $1000$  to  $1200\text{ cm}^{-1}$  frequency window was observed. A series of  
27 peaks in this window were observed to coincide with peak positions that have been assigned  
28 to arise from defects on the nanotubes surface. We find that these peaks also occur for  
29 chemically treated SWCNTs.  
30  
31  
32  
33  
34

## 35 2. Experimental

36 SERRS measurements were carried out with a single monochromator (Roper Acton SP2300s)  
37 and EMCCD (Andor IXON) in a backscattering configuration using a  $60\times$  objective to excite  
38 and collect the scattered light. The spectral resolution was  $>1.5\text{ cm}^{-1}$ . SERRS measurements  
39 were conducted with  $532\text{ nm}$  (Nd:YAG laser) excitation. The SERRS substrates consisted for  
40 a thin film of silver of  $40\text{ nm}$  in thickness which was deposited onto a glass slide. Following  
41 this silver nanoparticles were then deposited onto the substrate surface, carbon nanotubes  
42 where then deposited onto the silver substrate. This created the SERRS active support which  
43 the SWCNTs were dispersed at low concentration in ethanol (abs) by sonication, spray coated  
44 onto freshly prepared SERRS substrates and dried in a desiccator. Purified commercially  
45 sourced SWCNTs (p-SWCNTs) were purchased from Carbon Nanotechnologies, Inc. and  
46 used as supplied. Highly purified and selectively oxidised SWCNTs (o-SWCNTs) were  
47 prepared according to a recently published purification/oxidation protocol [4]. Briefly, this  
48 method involves a short nitric acid oxidation to minimize structural/electronic degradation of  
49 SWCNTs and sodium hydroxide treatments to remove carboxylated carbonaceous impurities.  
50 A hydrogen peroxide oxidization step efficiently etches remaining carbonaceous impurities  
51 and ensures full oxidation of oxygenated species to carboxylic acid moieties. Persistence of  
52 characteristic optical properties indicating the preservation of the electronic structure during  
53 chemical treatment has been demonstrated [4]. Atomic Force Microscopy (AFM) images  
54 were recorded using an explorer AFM system.  
55  
56  
57  
58  
59  
60  
61  
62  
63  
64  
65

### 3. Results and discussion

SERRS and Raman spectra of p-SWCNT are shown in Fig. 1. Fig 1a shows SERRS spectra of p-SWCNTs recorded sequentially with a 10 s interval as an intensity plot. The SERRS spectra show temporally fluctuating peaks superimposed on the G and D band regions. Areas of the sample that show the presence of these fluctuating peaks are found randomly across the sample with some regions of the sample showing no sharp fluctuating peaks, only broadened G and D bands with stable profiles. Fig 1b shows two SERRS spectra taken from different regions of the sample. One spectra show broadened G and D band features, the second spectrum shows sharp features within the G and D band region. The G and D modes are broadened compared to the Raman spectra. Broadening of the G and D band regions in SWCNT has been reported to occur for nanotubes on thin (c.a. >20 nm) silver films [16]. Fig 1c shows a sequence of ten spectra recorded over a concurrent period of p-SWCNTs. Fluctuating peaks are seen in this spectral sequence with band positions and band intensities changing. Carbon nanotubes possess strong Raman scattering cross sections which when coupled with plasmonic enhancement enables small number of nanotubes to be observed down to the single nanotube level. The effect of ensemble averaging potentially gives rise to temporal fluctuations of intensities and frequencies. With SWCNTs of different sizes and orientations been observed at different times creating temporally fluctuating spectral signals.

In order to assess the type of nanotube probed a study of the radial breathing mode (RBM) region was undertaken. Fig 1d and e shows the RBM region of the SERRS spectrum. The spectrum recorded at 532 nm has peaks at 271, 240 and 188  $\text{cm}^{-1}$ . The RBM peak at 270  $\text{cm}^{-1}$  equates to a nanotube  $d_t = 0.92$  nm as calculated by the relation,  $\omega_{\text{RBM}} = 248/d_t$ , where  $\omega_{\text{RBM}}$  and  $d_t$  indicate the RBM frequency and tube diameter, respectively [12-13]. The band at 240  $\text{cm}^{-1}$  has a  $d_t = 1.03$  nm. The RBM peak at 192  $\text{cm}^{-1}$  has a  $d_t = 1.29$  nm. Using the Kataura plot the nanotubes excited at 532 nm (2.33 eV) are predominantly metallic nanotubes for p-SWCNT were all tubes c.a. <275  $\text{cm}^{-1}$  and >200  $\text{cm}^{-1}$  arise from metallic nanotubes and those above are from semiconducting tubes [17]. Maultzsch et al applied resonant Raman to study the radial breathing mode of nanotubes for more than 50 chiral indices with diameters between 0.6 and 1.5 nm [17]. The authors noted that  $\omega_{\text{RBM}} = 248/d_t + C$  is required to more correctly account for additional external forces, e.g., from interactions with a substrate or neighbouring tubes in a bundle. The silver SERRS active potential creates additional external forces on the nanotube thus requiring correction for estimation of the  $\omega_{\text{RBM}}$ , however it is noted that changes in the environment of the tubes probed so far lead to small changes in the RBM frequencies. Changing the excitation wavelength to 632 nm, changes also the RBM spectrum compared to the spectrum recorded at 532 nm. The spectra show that the p-SWCNT has a RBM peak at 283, 257 217 and 196  $\text{cm}^{-1}$ . These bands equate to metallic nanotubes for the bands <225  $\text{cm}^{-1}$  with the bands above this arising from semiconducting nanotubes. Thus on this basis the RBM spectra for p-SWCNT indicates that for 532 nm excitation predominantly metallic nanotubes are excited at 532 nm and predominantly semiconducting nanotubes are excited at 632 nm.

Fig 1d and e shows the RBM spectra for o-SWCNT recorded at 532 and 632 nm. The spectrum recorded at 532 nm has two peaks at 241 and 268  $\text{cm}^{-1}$ . The RBM peak at 241  $\text{cm}^{-1}$  equates to a nanotube  $d_t = 1.02$  nm as calculated by the relation,  $\omega_{\text{RBM}} = 248/d_t$  [12-13]. The band at 261  $\text{cm}^{-1}$  has a  $d_t = 0.95$  nm. Using the Kataura plot as above the nanotubes excited at 532 nm (2.33 eV) are predominantly metallic nanotubes for p-SWCNT were all tubes c.a. <275  $\text{cm}^{-1}$  and >200  $\text{cm}^{-1}$  arise from metallic nanotubes [17]. Changing the excitation wavelength to 632 nm, changes also the RBM spectrum compared to the spectrum recorded at 532 nm as for p-SWCNT. The spectra show that the o-SWCNT has a RBM peak at 282,

255 218 and 198  $\text{cm}^{-1}$ . These bands equate to metallic nanotubes for the bands  $<225 \text{ cm}^{-1}$  with the bands above this arising from semiconducting nanotubes. Thus on this basis the RBM spectra for p-SWCNT indicates that for 632 nm excitation predominantly from semiconducting nanotubes where when the nanotubes are excited at 532 nm predominantly metallic nanotubes are observed.

These sizes of nanotube can be related tentatively to nanotube chirality. Kurti et al using density functional theory obtained the geometrical properties and the radial breathing mode (RBM) frequency of a series of 40 different single-walled carbon nanotubes [18]. The authors predicted that a (9,9) nanotube would have a RBM peak at 192  $\text{cm}^{-1}$  and a (12,0) nanotube would have a RBM peak at 240  $\text{cm}^{-1}$ . However it is noted for example that there the assignment of the chirality of the nanotube at the diameter 1.3 nm can be made to several nanotubes such as (9,9) and also to (10,n) where  $n = 7, 8$  or 9. The broad RBM peaks potential possess a number of peaks corresponding to different nanotube chirality within this broad RBM envelop. Maultzsch et al applied resonant Raman to study the radial breathing mode of nanotubes for more than 50 chiral indices with diameters between 0.6 and 1.5 nm [17]. The authors noted that  $\omega_{\text{RBM}} = 248/d_t + C$  is required to more correctly account for additional external forces, e.g., from interactions with a substrate or neighbouring tubes in a bundle. The silver SERRS active potential creates additional external forces on the nanotube thus requiring correction for estimation of the  $\omega_{\text{RBM}}$ , however it is noted that changes in the environment of the tubes probed so far lead to small changes in the RBM frequencies.

Studies of defects in nanotubes such as STW have been performed by Fujimori et al and Vandescuren et al [7,8]. Fujimori et al reported temporally fluctuating SERRS spectra from SWCNTs with peaks in the D and G band regions and also peaks outside this region at 1139 and 1184  $\text{cm}^{-1}$  which were assigned to dynamic reconstruction of defective structures of SWCNTs arising from STW defects in the vicinity of SERRS-active sites under irradiation of the laser light [8]. This study was based on semiconductor nanotubes with diameters of c.a. 1.5 and 1.3 nm. Theoretical calculations by Vandescuren et al predicted Raman peaks for STW defects for (10, m) (where m is an integer between 0 and 10) nanotubes and for heptagonal-pentagonal defects for (9,0) and (12,0) nanotubes [7]. The SERRS study here potentially probes both (10, m) and (12,0) nanotube type as evidenced by the RBM spectra (see above).

Fig 2 displays SERRS spectra, i to iii, selected from the spectra shown in Fig 2a. Spectra i and ii possess peaks at 1143  $\text{cm}^{-1}$  as well as peaks at 1186  $\text{cm}^{-1}$  both marked  $\alpha$ . These bands are outside of the D and G wavelength region. The presence of the  $\alpha$  bands is accompanied by a strong band in the G band region at c.a. 1590  $\text{cm}^{-1}$ . Fig 2b shows that the bands marked  $\alpha$  are persistent over seconds. Analysis of the spectral features in Fig 2a show the presence of a band at 1270  $\text{cm}^{-1}$  (marked  $\beta$ ). Spectrum iii in Fig 2a does not possess spectral features at  $\alpha$  or  $\beta$ . Peaks (marked  $\chi$ ) are seen at 1276 and 1310  $\text{cm}^{-1}$ .

The intensity of several peaks as a function of time was assessed by plotting band intensity vs. time over a 250 sec interval (as shown in Fig 2c). Inspection of Fig 2c shows that the bands at 1142 and 1186  $\text{cm}^{-1}$  (assigned to STW defects) show similar fluctuations in Raman signal intensity with time. The band at 1270  $\text{cm}^{-1}$  can also be assigned to arise from STW defects and shows a similar fluctuation in Raman signal intensity over time compared to the bands at 1142 and 1186  $\text{cm}^{-1}$ . Looking at the Raman intensity over time for a band at 1599  $\text{cm}^{-1}$ , which is associated with a SWCNT G mode, the intensity fluctuations visible differ to the bands associated with STW defects. Calculating the Pearson product-moment correlation

1 coefficient  $r$  for the intensity allows for analysis of the ‘randomness’ in the intensity of peaks  
 2 [19]. Values close to zero indicate a random intensity variation while large values present a  
 3 strong linear correlation. The Pearson product-moment correlation coefficient for the  
 4 fluctuations in the  $\alpha$  peak at  $1183\text{ cm}^{-1}$  over the observed time-frame was as calculated to be  $r$   
 5  $= 0.27$ . This indicates that the intensity variation is random over the recorded time window.  
 6 Pearson product-moment correlation coefficient was employed to calculate the correlation  
 7 between two Raman peaks by comparing the Raman signal intensities as a function of time  
 8 i.e. when comparing two peaks. The variation of peak intensity of the two peaks at  $1183$  and  
 9  $1142\text{ cm}^{-1}$  yields a correlation coefficient  $r = 0.98$ . This value demonstrates a strong  
 10 correlation between the two Raman bands. Both bands are predicted to arise from STW  
 11 defects. Another band that was predicted to be associated with STW defects is the band at  
 12  $1270\text{ cm}^{-1}$ . Comparing the peaks at  $1142\text{ cm}^{-1}$  with the band at  $1270\text{ cm}^{-1}$  revealed a strong  
 13 correlation  $r = 0.94$ . This supports the assertion that the peaks at  $1270\text{ cm}^{-1}$  is associated with  
 14 STW defects. A relatively minor correlations ( $r = 0.47$  and  $0.46$  respectively) were found  
 15 between the STW peaks at  $1142$  or  $1183\text{ cm}^{-1}$  when compared to the peak at  $1598\text{ cm}^{-1}$  which  
 16 is associated with the G band in SWCNTs.  
 17  
 18  
 19  
 20

21 Fig 3 outlines the variation in Raman frequencies and intensities recorded for p-SWCNTs  
 22 recorded at  $632\text{ nm}$ . Fig 3a shows ten spectra recorded successively. Fig 3b shows the un-  
 23 normalized spectra as shown in Fig 3a. The spectra show the presence of fluctuating peaks  
 24 and a changing intensity in the spectral features. Magnifications of three spectra from Fig 3a  
 25 are displayed in Fig 3c. The upper spectrum in Fig 3c shows peaks at  $1144$  and  $1185\text{ cm}^{-1}$   
 26 (marked  $\alpha$ ). A band at  $1269\text{ cm}^{-1}$  (marked  $\beta$ ) is observed. These peaks are in the same  
 27 position as the bands observed at  $532\text{ nm}$  excitation. On this basis these peaks are assigned to  
 28 dynamic reconstruction of defective structures of SWCNTs arising from STW defects in the  
 29 vicinity of SERRS-active sites under irradiation of the laser light [8]. A small shift from  
 30  $1139$  to  $1143\text{ cm}^{-1}$  or  $1184$  to  $1186\text{ cm}^{-1}$  is present however. Theoretical calculations by  
 31 Vandescuren et al predicted further Raman peaks for STW defects at  $1270$  and  $1020\text{ cm}^{-1}$  [7].  
 32 The peak positions and intensities predicted by Vandescuren et al was for (10, m) SWCNT  
 33 [7]. Analysis of the spectral features in Fig 2 and 3 show the presence of a band at  $1270\text{ cm}^{-1}$   
 34 (marked  $\beta$ ). While a band at  $1020\text{ cm}^{-1}$  does not clearly appear. However, it is noted that the  
 35 predicted band intensity at  $1020\text{ cm}^{-1}$  is much weaker than the predicted band intensity at  
 36  $1270\text{ cm}^{-1}$ . Spectra in Fig 2 and 3 also can show peaks (marked  $\chi$ ) at  $1276$  and  $1310\text{ cm}^{-1}$ .  
 37 These bands can be assigned, on the basis of theoretical calculations by Vandescuren et al, to  
 38 heptagonal-pentagonal intramolecular junctions in carbon nanotubes, which correspond to  
 39 defect modes localized on the pentagon and slightly around it [7]. These bands are reported to  
 40 occur at  $1275$  and  $1315\text{ cm}^{-1}$ .  
 41  
 42  
 43  
 44  
 45

46 Fig 4 outlines the variation in Raman frequencies and intensities recorded for o-SWCNTs  
 47 recorded at  $632\text{ nm}$ . Fig 4a shows ten spectra recorded successively. Fig 4b shows  
 48 normalized spectra as shown in Fig 4a. The spectra show the presence of fluctuating peaks  
 49 and a changing intensity in the spectral features. The upper spectrum possesses peaks at  $1143$   
 50  $\text{cm}^{-1}$  as well as peaks at  $1186\text{ cm}^{-1}$  both marked  $\alpha$ . Analysis of the spectral features shows  
 51 also the presence of a band at  $1270\text{ cm}^{-1}$  (marked  $\beta$ ). The lower spectrum in Fig 4a does not  
 52 possess spectral features at  $\alpha$  or  $\beta$ . Peaks (marked  $\chi$ ) are seen at  $1276$  and  $1310\text{ cm}^{-1}$ . These  
 53 bands are in the same position and possess similar relative intensities are the bands marked  
 54 correspondingly for p-SWCNT excited at  $632\text{ nm}$  (as shown in Fig 3). This shows the  
 55 treatment to produce the oxidised SWCNT (o-SWCNT) does not change the presence of  
 56 bands potentially arising from defect sites.  
 57  
 58  
 59  
 60  
 61  
 62  
 63  
 64  
 65

1 The substrate was analysed using microscopy. Fig 5a shows an AFM microscopy image  
2 recorded of the SWCNTS on a glass slide. The dispersed sample shows the presence of  
3 aggregates on the sample surface containing few nanotubes. The presence of single nanotubes  
4 was not definitively found due to a combination of the small size of these structures making it  
5 difficult for the AFM to image them. Images of the carbon nanotubes were obtained on a  
6 cleaned glass slide to determine their dispersion, whereby the glass forms a smooth surface.  
7 The distribution of the nanotubes was seen to be inhomogeneous across the sample surface.  
8 The presence of aggregates of nanotubes and the inhomogeneous distribution of silver on the  
9 substrate indicates that there is expected to be a variation in the Raman spectral features  
10 expected when probing a small area of the sample. The use of a high powered objective (ie  
11 60X) enables the probing of areas of the sample on the few micron length scales. The  
12 inhomogeneous distributions of plasmonic active silver and nanotube dispersion explains the  
13 occurrence of some regions of the sample randomly occurring as you scan the sample that  
14 show temporal fluctuations in the SERRS spectra. The inset shows an optical reflection  
15 contrast image of the substrate. The image in Fig 5a shows a selection of the sample area of  
16 the silver film substrate which has present on its surface deposited silver nanoparticles, which  
17 were deposited after the silver film was made. The image shows that the silver is not a  
18 continuous film but is fragmented in into small and large areas or islands on the substrate on  
19 length scales on the scale of microns or larger. This means that the silver substrate is an  
20 inhomogeneous plasmon active substrate layer on which the carbon nanotubes are located.  
21 AFM studies were undertaken of the samples surface to enable more spatially resolved  
22 information to be obtained. Fig 5b show an AFM topography image of the surface features of  
23 the silver film which the SWCNTs are deposited onto. Inset i) shows a potential observation  
24 of SWCNTS on the substrate. An inhomogeneous surface topography was found. The  
25 topography profile plot (inset ii) indicates that certain regions of the samples surface are  
26 rough on the order of 100's of nm and others rough on the length scale of 10's of nm. 'Hot  
27 spot' areas of high plasmon enhancement may be present on this sample as a result of the  
28 fragmentation of the silver on the >micron length scale, in addition to the presence of the nm  
29 roughed surface features as a result of the presence of silver nanoparticles. This nm sized  
30 roughness potentially can create plasmon enhancement 'hot spots'. Fluctuations in the  
31 SERRS Raman band intensities and positions have been observed previously and have been  
32 proposed to arise from the presence of such create plasmon enhancement "hot spots" on  
33 SERRS-active metals such as silver.  
34  
35  
36  
37  
38  
39  
40

41 Molecular dynamic simulations were undertaken using MM+ methodology. The simulation  
42 was based on silver ions and a nanotube structure. The ions were calculated to interact with  
43 the nanotube. The ions were found to enter the nanotube and assemble with the nanotube and  
44 around its external structure, were the silver was placed at the beginning of the calculation.  
45 This simulation provides evidence that the silver ions are in proximity to the nanotube surface  
46 and as a consequence may interact with defect sites such as a mobile STW defect that may be  
47 present from a vacancy in the tube. The presence of these silver ions potentially influence the  
48 nanotubes structure and in turn the resulting Raman spectra. In addition it is noted that the  
49 presence of the nanoscale rough silver environment may lead to restricting the vibration  
50 motion of the nanotube leading to in turn a change in the frequency and intensity of the  
51 resulting Raman. The observed SERRS temporal Raman spectral features may result from a  
52 perturbation of the Raman modes and not by the presence of defects.  
53  
54  
55  
56

57 o-SWCNTs are prepared from p-SWCNTs using acid based treatment, creating the addition  
58 of oxide groups at the end of the nanotubes or in areas of vacancies in the nanotubes surface.  
59 The presence of the oxide groups do not remove the occurrence of bands associated with  
60  
61  
62  
63  
64  
65

1 STW defects. The observed SERRS spectrum is modified compared to the Raman spectra for  
2 both the p-SWCNT and o-SWCNT as evidenced by the large D band SERRS intensity  
3 compared to the spectral features for the resonance Raman spectral features [ref]. The intense  
4 D band in the SERRS indicates a change in the degree of disorder. The D band in the SERRS  
5 increases its intensity and displays a change in profile. The broadening of the D and G band  
6 region has been assigned to an interaction between the silver and the nanotube centring on the  
7 charge transfer mechanism responsible (in part) for the SERRS enhancement [16]. The  
8 presence of the silver nanoparticle layer potentially contributes also to this broadening and  
9 enhancement of the D band region.  
10

11 Photo-induced structural changes such as the decomposition of the nanotube can potentially  
12 lead to the observation of bands in the c.a.  $1150\text{ cm}^{-1}$  region assigned to STW defects as  
13 outlined above. Lefrant et al showed that SERRS from SWCNT could be interpreted in terms  
14 of degradation of the single-walled nanotubes and the formation of particles similar to highly  
15 oriented pyrolytic graphite e.g.  $C_{60}$  and amorphous carbon [16]. Lefrant et al demonstrated  
16 that the presence of materials such as  $C_{60}$  is expected to result in Raman spectra with marker  
17 bands at  $1458\text{ cm}^{-1}$  [16]. No bands were observed at this position in the SERRS spectra  
18 indicating that the no  $C_{60}$  was formed. However the broad G and D bands seen in Fig 1b and  
19 3a indicates that there is strong coupling between the SWCNT and the silver substrate. This  
20 coupling is expected to lead to strong SERRS.  
21  
22  
23  
24  
25  
26

#### 27 4. Conclusion

28 SERRS studies on commercially available purified SWCNTs and oxidized SWCNTs have  
29 been carried out. For both samples SERRS spectra with and without temporal fluctuations in  
30 peak frequencies and intensities were found depending upon the area probed. The origin for  
31 the SERRS spectra with temporal fluctuations in peak frequencies and intensities was  
32 ascribed to single and/or few nanotubes been located in regions of the sample that possessed  
33 high plasmon localisation. Areas of relatively high and low plasmon localisation result from  
34 the rough surface topography of the silver substrate. In p-SWCNTs and o-SWCNT temporal  
35 fluctuating peaks in the region between  $1000$  to  $1350\text{ cm}^{-1}$  Raman shift have been ascribed to  
36 the dynamic behaviour of STW and heptagonal-pentagonal intramolecular junction defects  
37 based on comparing the band positions observed to simulated values for the occurrence of  
38 such defects in nanotubes. Evidence for carbonaceous impurities photochemically generated  
39 in the sample was not definitively found, e.g. no occurrence of Raman bands at c.a.  $1458\text{ cm}^{-1}$   
40 (definitive for  $C_{60}$ ) was observed when Raman bands for STW defects were observed. The  
41 effect of chemical introduction of carboxylic acid moieties to the surface of the nanotubes  
42 was seen to alter the spectral profile in the frequency region associated with bands arising  
43 from of Stone-Thrower-Wales and heptagonal-pentagonal intramolecular junction defects in  
44 the nanotube.  
45  
46  
47  
48  
49  
50

51 The treatment that creates the o-SWCNT nanotubes potentially can lead to a covalent bond  
52 occurring at a defect site. The occurrence of bands that can be assigned to defect sites  
53 indicates that the presence of oxides on the nanotube does not remove the defects. In addition  
54 the occurrence of strong D band intensities indicates further that potentially disorder/defects  
55 may be present on the nanotubes surface. MM+ calculations show that silver ions may be  
56 present within the tubes structure as well as near its external wall structure, these ions  
57 potentially perturbing the nanotubes structure and Raman spectral features. While the  
58 presence of photo-induced decomposition cannot be ruled out and also potentially impurities  
59  
60  
61  
62  
63  
64  
65

1 from the atmosphere or from contamination elsewhere may explain the observed bands, the  
2 occurrence of bands in the positions labelled  $\alpha$  and  $\beta$  have been calculated to occur from  
3 defects in grapheme. Furthermore the calculations by Fujimori et al were performed on a  
4 sheet which is applicable to nanotubes of different sizes and chirality.

## 7 **Acknowledgment**

8  
9 The authors acknowledge Science Foundation Ireland (PIYRA 07/YI2/I1052), IRCSET and  
10 Intel (postdoctoral fellowship to IK) for support. We acknowledge the support from the Iraq  
11 government for their postgraduate studentship for Nebras Al-Altar. We are grateful to Dr.  
12 Kevin Flavin for the o-SWCNTs. The authors are also grateful for the work of Alexei  
13 Kudryashov in data analysis.  
14  
15

## 17 **References**

- 18  
19 1. M.S. Dresselhaus, G. Dresselhaus, P. Avouris, Carbon Nanotubes: Synthesis, Structure,  
20 Properties and Applications, Springer Series in Topics in Applied Physics Vol. 80 (Springer-  
21 Verlag, Berlin) 2001.  
22  
23
- 24 2. K. Flavin, K. Lawrence, J. Bartelmess, M. Tasiar, C. Navio, C. Bittencourt, D. O' Shea,  
25 D.M. Guldi, S. Giordani, ACS Nano, 5 (2001) 1198.  
26  
27
- 28 3. Kevin Flavina, Ilona Kopfa, Cristina Naviob, Carla Bittencourtb, and Silvia Giordani. ACS  
29 Nano. in press, 2011.  
30  
31
- 32 4. K. Flavin, I. Kopf, E. Del Canto, C. Navio, C. Bittencourt, S. Giordani, "Controlled  
33 carboxylic acid introduction: a route to highly purified oxidized single walled carbon  
34 nanotubes" J. Mat. Chem., 2011. DOI:10.1039/C1JM12217G  
35  
36
- 37 5. A.J. Stone, D.J. Wales, Chem. Phys. Lett. 128 (1986) 501.  
38  
39
- 40 6. M. Ouyang, J.L. Huang, C.L. Cheung, C.M. Lieber, Science 291 (2001) 97.  
41  
42
- 43 7. M. Vandescoren, H. Amara, R. Langlet, P. Lambin. Carbon, 45 (2007) 349.  
44  
45
- 46 8. T. Fujimori, K. Urita, T. Ohba, H. Kanoh, K. Kaneko, J. Am. Chem. Soc., 132 (2010)  
47 6764.  
48  
49
- 50 9. H.F. Bettinger, J. Phys. Chem. B, 109 (2005) 6922.  
51  
52
- 53 10. M.B. Nardelli, B.I. Yakobson, J. Bernholc, Phys. Rev. Lett, 81 (1998) 4656.  
54  
55
- 56 11. F. Lordan, J.H. Rice, B. Jose, R.J. Forster, T.E. Keyes. Appl. Phys. Lett., 99 (2011)  
57 033104.  
58  
59
- 60 12. K. Kneipp, L.T. Perelman, H. Kneipp, V. Backman, A. Jorio, G. Dresselhaus, M.S.  
61 Dresselhaus, Phys. Rev. B, 63 (2001) 193411.  
62  
63  
64  
65

- 1  
2  
3  
4  
5  
6  
7  
8  
9  
10  
11  
12  
13  
14  
15  
16  
17  
18  
19  
20  
21  
22  
23  
24  
25  
26  
27  
28  
29  
30  
31  
32  
33  
34  
35  
36  
37  
38  
39  
40  
41  
42  
43  
44  
45  
46  
47  
48  
49  
50  
51  
52  
53  
54  
55  
56  
57  
58  
59  
60  
61  
62  
63  
64  
65
13. K. Kneipp, H. Kneipp, M. S. Dresselhaus, S. Lefrant, Phil. Trans. R. Soc. Lond. A, 362 (2004) 2361.
14. Y. Zhang, H. Son, J. Zhang, M. S. Dresselhaus, J. Kong, Z. Liu. J. Phys. Chem. C, 111 (2007) 1983.
15. Y. Miyamoto, A. Rubio, S. Berber, M. Yoon, D. Tomanek. Phys. Rev. B. 69 (2004) 121413.
16. S. Lefrant, I. Baltog, M. Baibarac, J. Schreiber, O. Chauvet. Phys Rev B, 65 (2002) 235401.
17. J. Maultzsch, H. Telg, S. Reich, C. Thomsen, Phys. Rev. B. 72 (2005) 205438.
18. J. Kurti, V. Zolyomi, M. Kertesz, G. Sun, New J. Phys., 5 (2003) 125.1
19. J.H. Rice, J.W. Robinson, A. Joujour, R.A. Taylor, R. Oliver, G.A.D. Briggs. Appl Phys Letts, 84(2004) 41101.

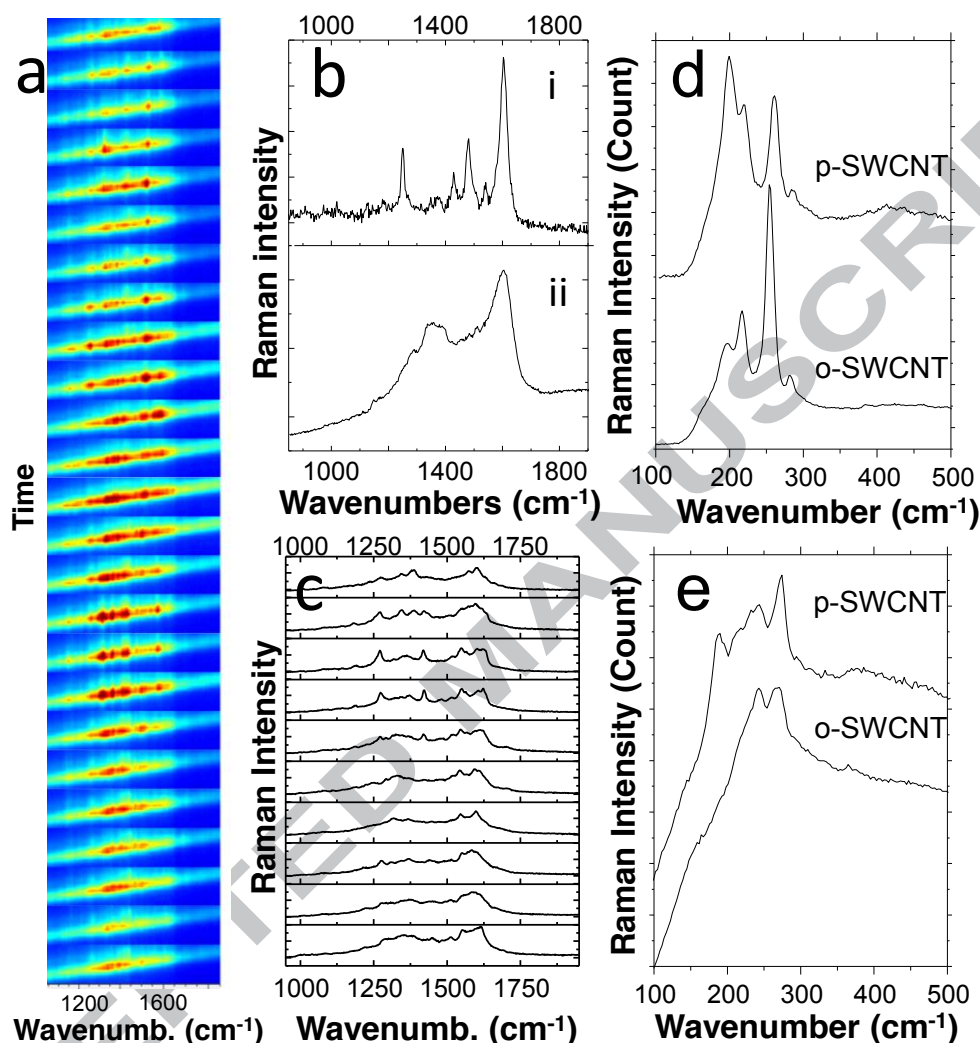


Fig 1. a) Temporally fluctuating SERRS spectra of p-SWCNTs.  $\lambda_{\text{excitation}} = 532$  nm. The power density was  $0.65 \text{ MW cm}^{-2}$ . Each SERRS spectrum was acquired for 1s with a time interval of 10s. A series of SERRS spectra recorded consequently. Note the tilt in the spectra shown is accounted for in extracting the data shown in following figures c). b) SERRS spectra taken at different regions of the sample. i) show a region where no temporal variation in band intensities are seen and ii) a region of the sample showing variation in the spectral profile over time. c) Shows ten spectra taken from the series shown in a), the band intensities have been normalised for clarity. d) and e) SERRS spectra in the RBM spectral region.

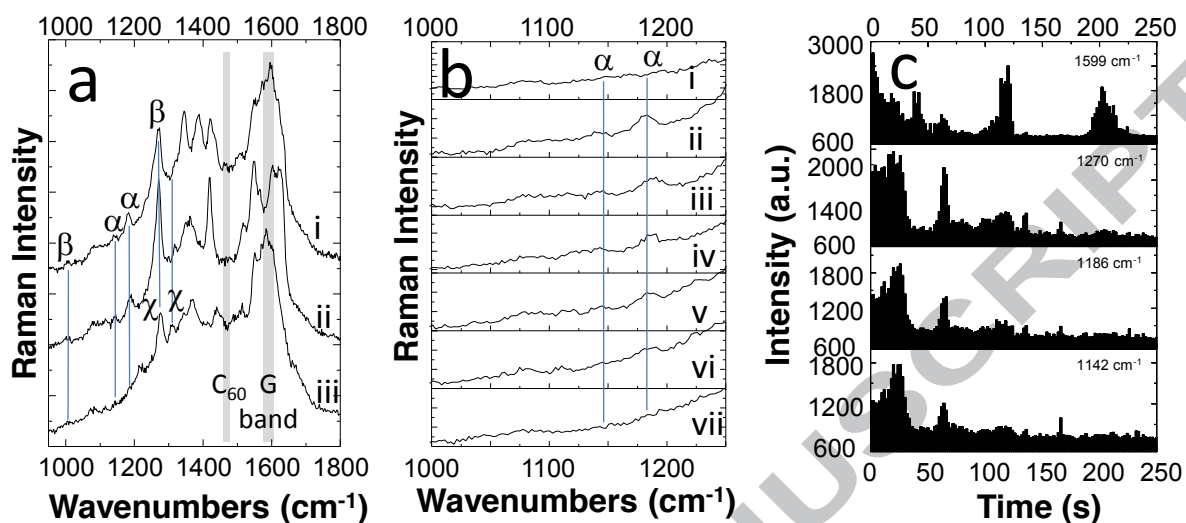


Fig 2. Temporally fluctuating SERRS spectra of p-SWCNTs.  $\lambda_{\text{excitation}} = 532 \text{ nm}$ . The power density was  $0.65 \text{ MW cm}^2$ . Each SERRS spectrum was acquired with a time interval of 10s. a) shows three spectra taken from Fig 1c,  $\alpha$ ,  $\beta$  and  $\chi$  mark band positions. b) shows magnified sections of the spectra shown Fig 1d, the band intensities have been normalised for clarity. c) a plot of peak intensity vs time for temporally fluctuating SERRS peak intensities acquired with a time interval of 2s as a function of time over 250 s.

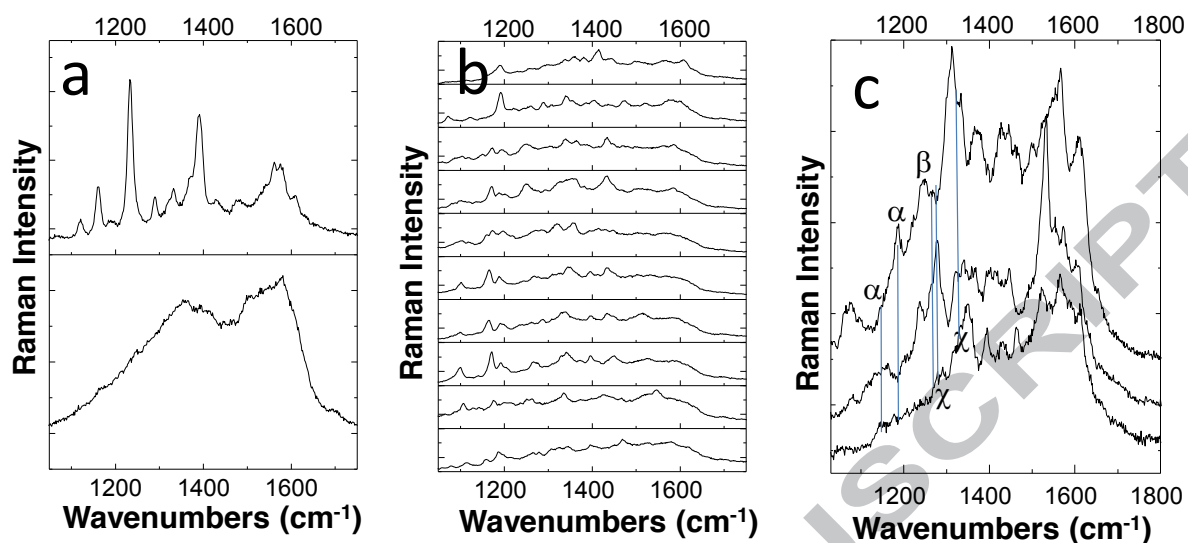


Fig 3. Temporally fluctuating SERRS spectra of p-SWCNTs.  $\lambda_{\text{excitation}} = 632 \text{ nm}$  Each SERRS spectrum was acquired with a time interval of 10s. The power density was  $0.65 \text{ MW cm}^{-2}$ . The spectra are normalized for clarity. a) Two spectra taken from different parts of the sample. b) a series of ten spectra taken consecutively. c) Three spectra were taken from Fig 3a shown for clarity.

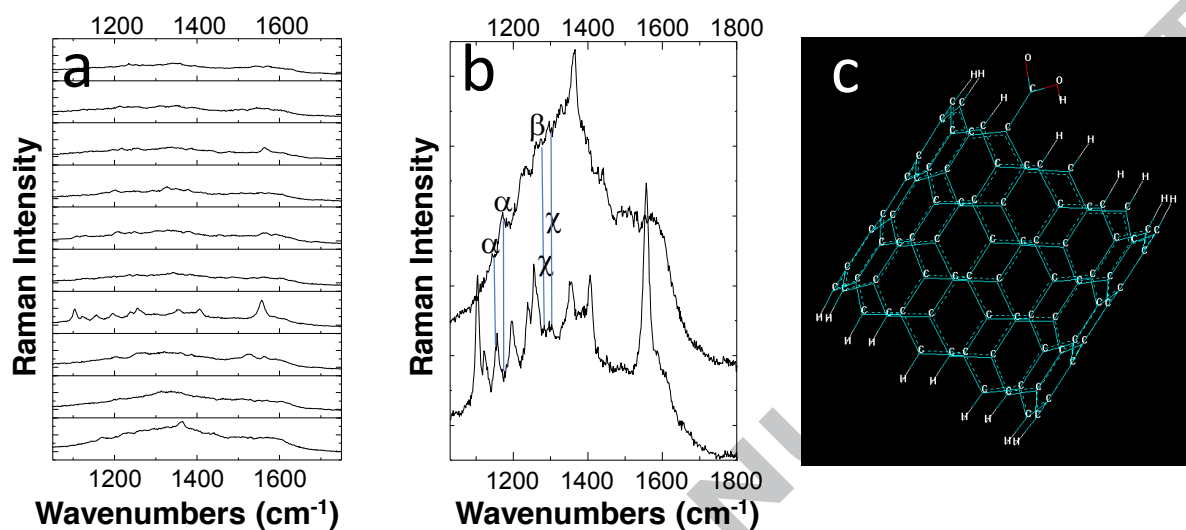


Fig 4. a) Temporally fluctuating SERS spectra of o-SWCNTs.  $\lambda_{\text{excitation}} = 632 \text{ nm}$  Each SERS spectrum was acquired with a time interval of 10s. The power density was  $0.65 \text{ MW cm}^{-2}$ . The spectra are normalized for clarity. b) Two spectra were taken from Fig 3a shown for clarity. c) Schematic drawing of o-SWCNT, the COOH group attached at the end of the nanotube.

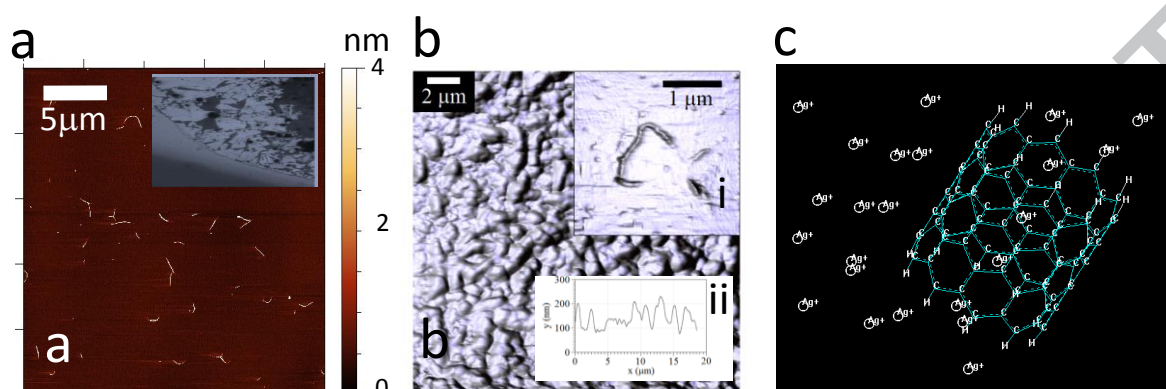
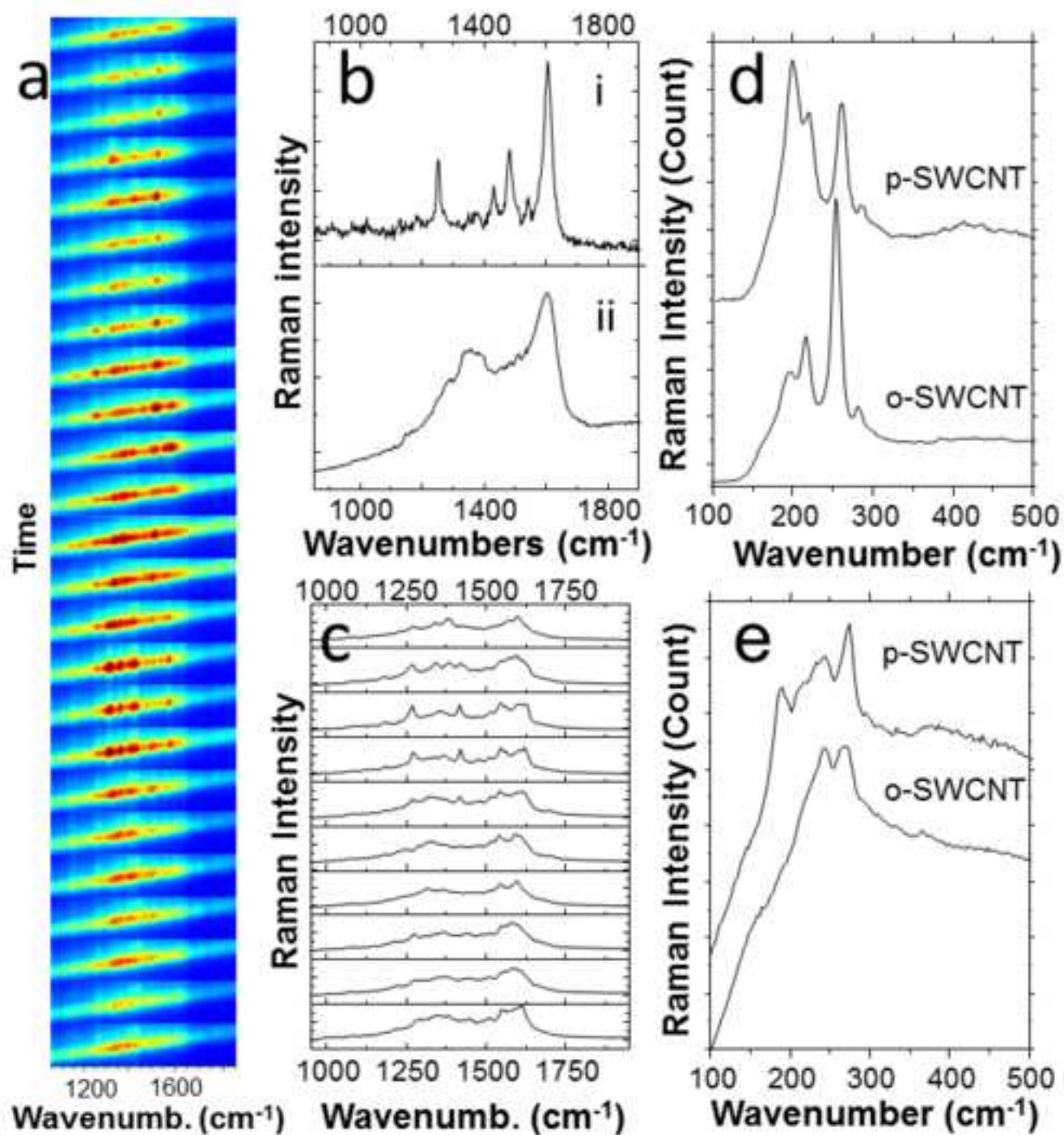
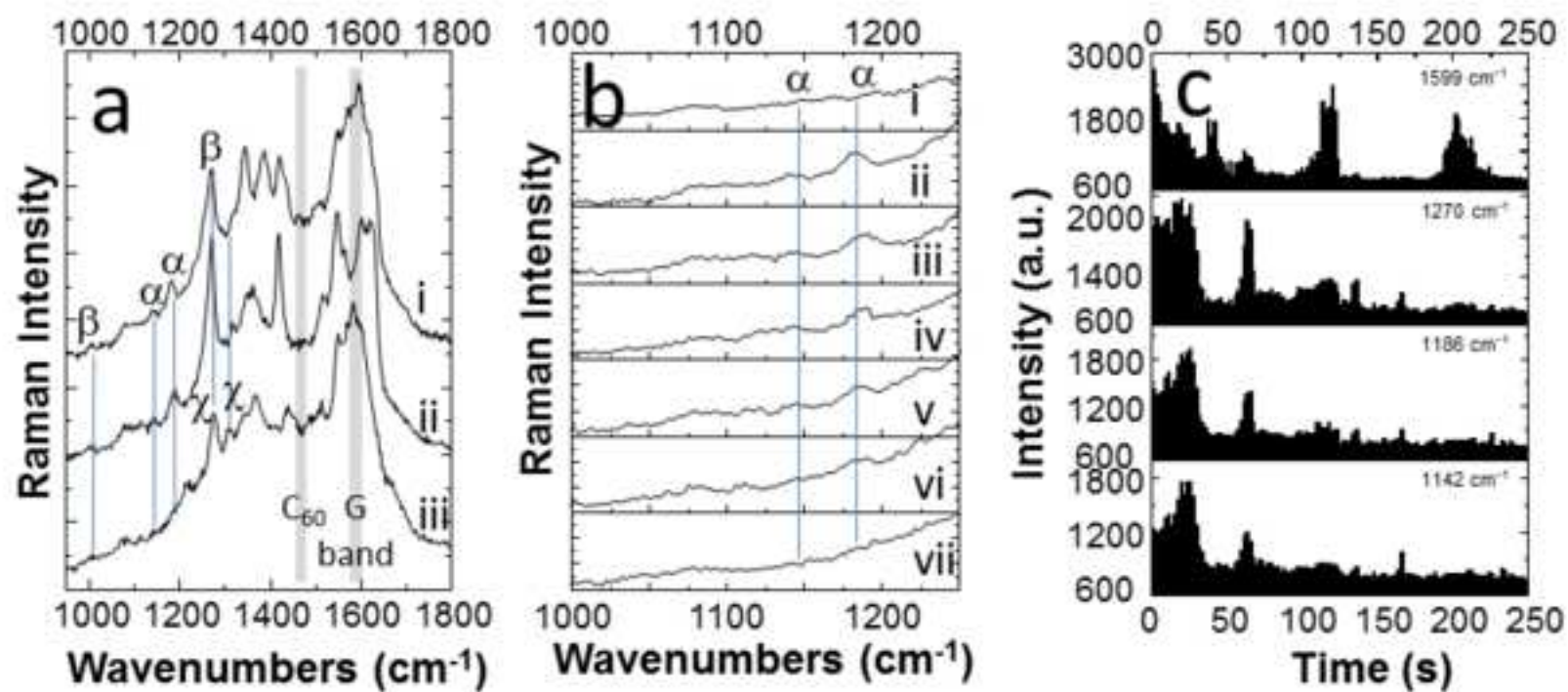
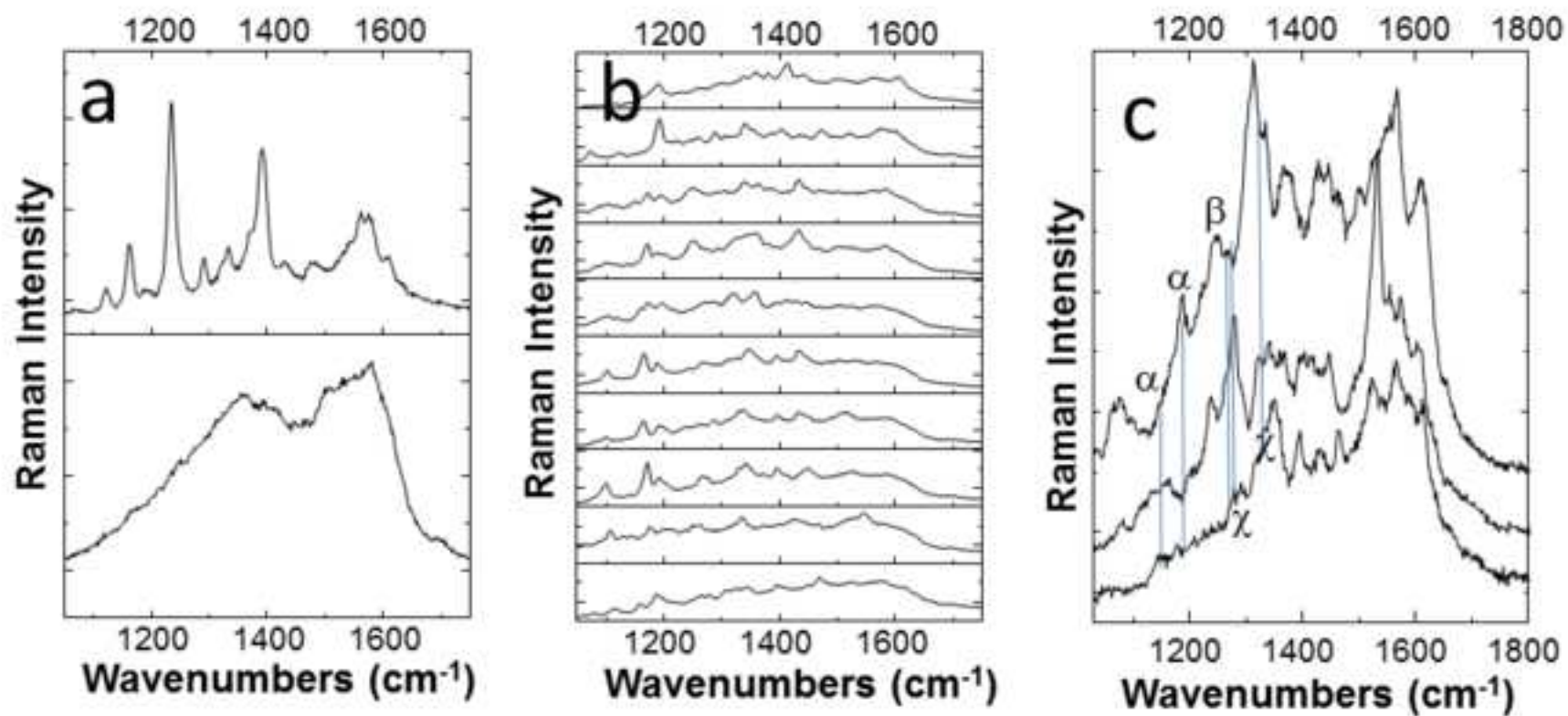
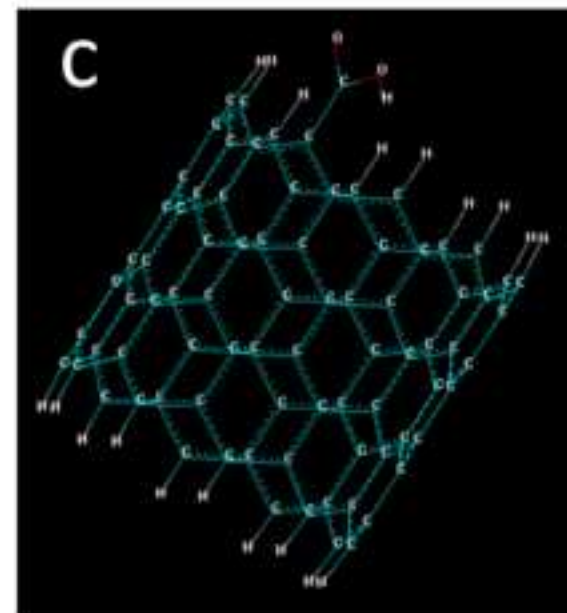
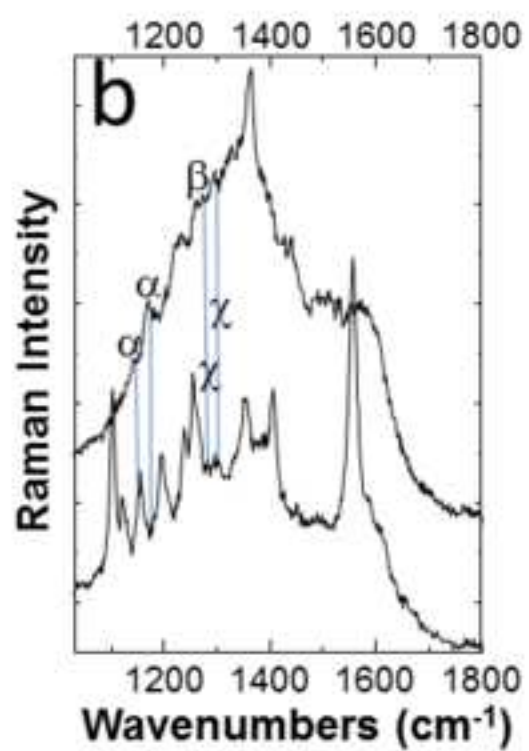
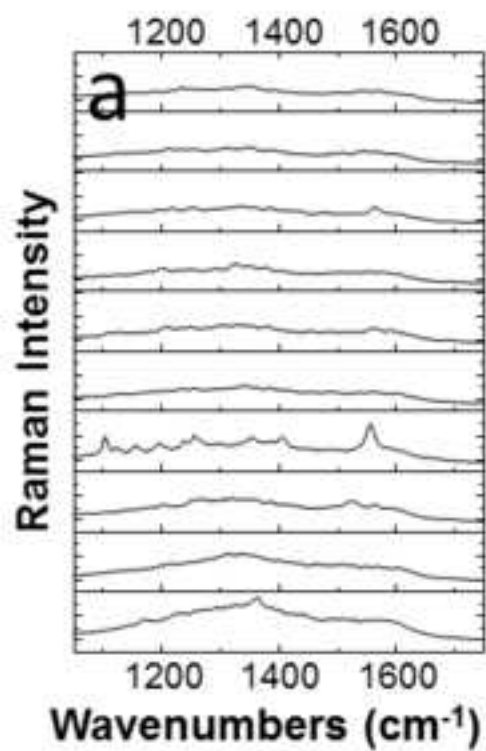


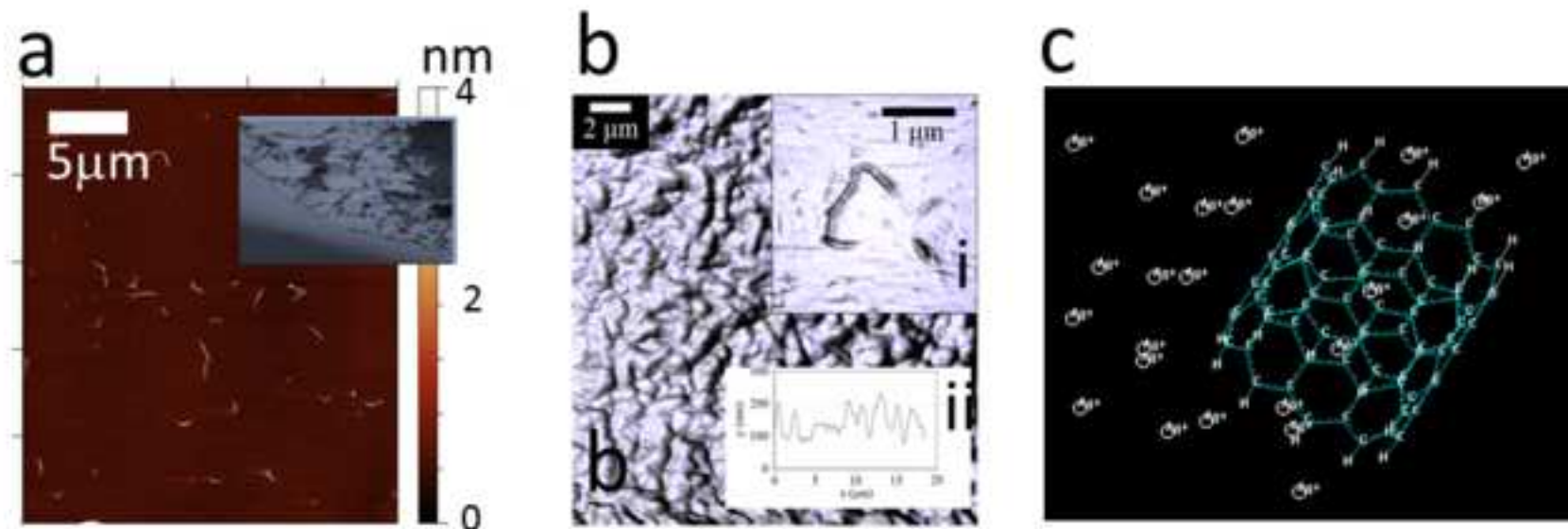
Fig 5. a) AFM topography image of o-SWCNTs dispersed onto a glass slide, using the same dispersion methods employed to prepare all the samples studied. The AFM image showing features in white which are assigned to arise potentially from clusters of carbon nanotubes c.a. 4 nm in height (from the background substrate) present on the substrates surface. These clusters potentially containing few nanotubes where 1 nanotube is c.a. 1 nm in height and potentially microns in length. The presence of single nanotubes was not definitively found. The inset shows an optical reflection contrast images of the sample surface of the silver film following the addition of silver nanoparticles. The images were recorded with a standard CMOS camera mounted onto a AFM system. b) AFM topography image of the substrate surface. The inset ii) shows a AFM topography profile plot showing that the roughness of the silver film is inhomogeneous with a parts of the sample surface been rough on the order of 100 nm and others been on the order of 10's of nm. inset ii) shows features associated with SWCNTS on the silver surface. The topography image shows features associated with SWCNT present on the silver surface, noting that only a relatively smooth part of the surface enabled features assigned to SWCNTs to been seen. c) Molecular dynamics simulation of the interaction of silver ions and a nanotube structure.

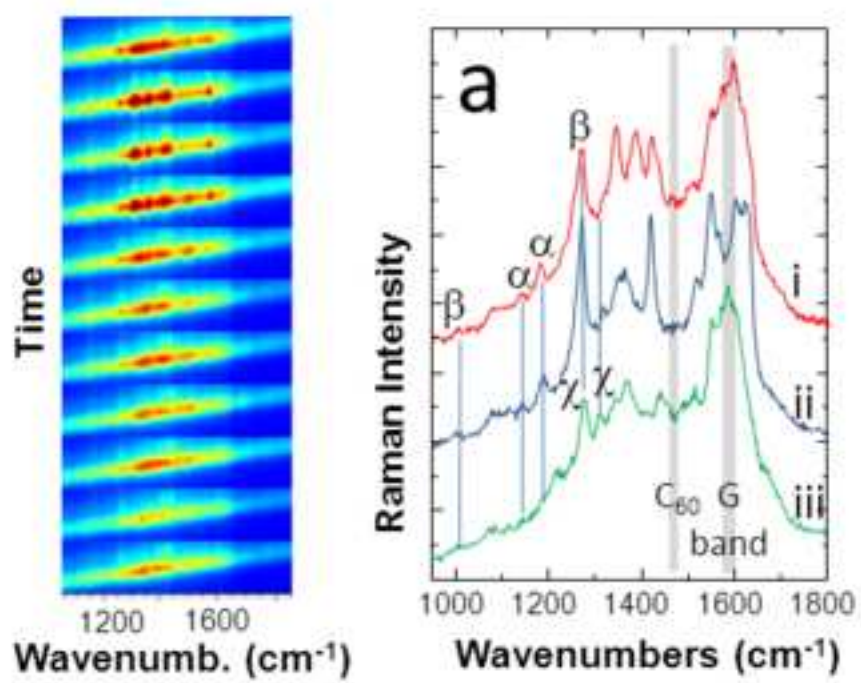














UCD School of Physics  
Science Center - North  
University College Dublin  
Belfield, Dublin 4, Ireland  
T +353 1 716 2213  
F +353 1 283 7275

Scoil na Fisice UCD  
Ionad Eolaíochta - Thuaidh  
An Coláiste Ollscoile, Baile Átha Cliath  
Belfield, Baile Átha Cliath 4, Éire  
[www.ucd.ie/physics](http://www.ucd.ie/physics)

James Rice  
School of Physics,  
University College Dublin,  
Belfield, Dublin 4, Ireland.  
Phone +353 (0)1 716 2229

11 Feb 2012

### Highlights

Surface-enhanced Raman scattering spectra of purified and oxidised single walled carbon nanotubes

Potential evidence for the presence of Stone-Thrower-Wales and heptagonal-pentagonal intramolecular junction defects.

Effect of chemical introduction of carboxylic acid moieties to the surface of the nanotubes